© 2021. This manuscript version is made available under the CC-BY-NC-ND 4.0 license http://creativecommons.org/licenses/by-nc-nd/4.0/
The published version is available via https://doi.org/10.1016/j.bbadis.2021.166236.

Extracellular vesicles of *P. gingivalis*-infected macrophages induce lung injury

Kayo Yoshida[a], Kaya Yoshida[b]*, Natsumi Fujiwara[a], Mariko Seyama[a], Kisho Ono[c], Hotaka Kawai[d], Jiajie Guo[e, f], Ziyi Wang[g], Yao Weng[f], Yaqiong Yu[e, f], Yoko Uchida-Fukuhara[f], Mika Ikegame[f], Akira Sasaki[c], Hitoshi Nagatsuka[d], Hiroshi Kamioka[g], Hirohiko Okamura[f], Kazumi Ozaki[a]

[a]Department of Oral Healthcare Promotion, Institute of Biomedical Sciences, Tokushima University Graduate School, Tokushima, Japan.
[b]Department of Oral Healthcare Education, Institute of Biomedical Sciences, Tokushima University Graduate School, Tokushima, Japan.
[c]Department of Oral and Maxillofacial Surgery and Biopathology, Graduate School of Medicine,
[d]Department of Oral Pathology and Medicine, Graduate School of Medicine, Dentistry and Pharmaceutical Sciences, Okayama University, Okayama, Japan.
[e]School and Hospital of Stomatology, China Medical University, Liaoning Provincial Key Laboratory of Oral Diseases, Shenyang, China.
[f]Department of Oral Morphology, Graduate School of Medicine, Dentistry and Pharmaceutical Sciences, Okayama University, Okayama, Japan.
[g]Department of Orthodontics, Graduate School of Medicine, Dentistry and Pharmaceutical Sciences, Okayama University, Okayama, Japan.

*Address correspondence to:
Kaya Yoshida, DDS, Ph.D.
3-18-15, Kuramoto, Tokushima 770-8504, Japan.
TEL: 81-88-633-7898, FAX: 81-88-633-7898; E-mail: kaya@tokushima-u.ac.jp
ORCID ID: https://orcid.org/0000-0002-3202-0634

Highlights

- *P. gingivalis* (*Pg*)-infected macrophages release extracellular vesicles (EVs).
- Histone H3 were existed in EVs derived from *Pg*-infected macrophages (*Pg*-inf EVs).
- *Pg*-inf EVs were transferred to the lungs, liver, and kidneys of mice.
- *Pg*-inf EVs induced inflammation and alveolar destruction in mice.
- *Pg*-inf EVs or Histone H3 promoted inflammation via the NF-κB pathway in A549 cells.

Abstract

Periodontal diseases are common inflammatory diseases that are induced by infection with periodontal bacteria such as *Porphyromonas gingivalis* (*Pg*). The association between periodontal diseases and many types of systemic diseases has been demonstrated; the term "periodontal medicine" is used to describe how periodontal infection/inflammation may impact extraoral health. However, the molecular mechanisms by which the factors produced in the oral cavity reach multiple distant organs and impact general health have not been elucidated. Extracellular vesicles (EVs) are nano-sized spherical structures secreted by various types of cells into the tissue microenvironment, and influence pathophysiological conditions by delivering their cargo. However, a detailed understanding of the effect of EVs on periodontal medicine is lacking. In this study, we investigated whether EVs derived from *Pg*-infected macrophages reach distant organs in mice and influence the pathophysiological status. EVs were isolated from human macrophages, THP-1 cells, infected with *Pg.* We observed that EVs from *Pg*-infected THP-1 cells (*Pg*-inf EVs) contained abundant core histone proteins such as histone H3 and translocated to the lungs, liver, and kidneys of mice. *Pg*-inf EVs also induced pulmonary injury, including edema, vascular congestion, inflammation, and collagen deposition causing alveoli destruction. The *Pg*-inf EVs or the recombinant histone H3 activated the NF-κB pathway, leading to increase in the levels of pro-inflammatory cytokines in human lung epithelial A549 cells. Our results suggest a possible mechanism by which EVs produced in periodontal diseases contribute to the progression of periodontal medicine.

Keywords: periodontal diseases, lung diseases, infection, inflammation, epithelial cells, animal experimentation

1. Introduction

Periodontal diseases are common inflammatory diseases induced by infection with periodontal bacteria, such as *Porphyromonas gingivalis* (*Pg*). The term "periodontal medicine" is used to describe how periodontal infection/inflammation may impact extraoral health. The association between periodontal diseases and many types of systemic diseases including diabetes mellitus [1, 2], rheumatoid arthritis [3], Alzheimer's disease [4] has been well demonstrated. Cytokine production and immune responses induced by a bacterial infection in periodontal tissue are considered to affect the development of periodontal medicine [5]. However, the molecular mechanisms by which the factors produced in the oral cavity reach multiple distant organs and affect general health have not been elucidated in detail.

Extracellular vesicles (EVs) are lipid bilayer-limited spherical structures with sizes ranging from 50 nm to 1 μm that are secreted from various types of cells into the environment [6]. EVs "cargo" contains components of donor cells such as proteins, nucleic acids, lipids, and metabolites [7]. The released EVs can pass through body fluids and transfer cargo to distant acceptor cells that regulate cell-to-cell and intercellular communications [8]. Therefore, EVs can influence various pathophysiological conditions such as cancer, immunity, metabolism, and neurodegeneration [9].

EVs appear to be secreted into periodontal tissue because the amount of EVs in the gingival crevicular fluid is increased in patients with periodontitis [10]. The gingival epithelial cells exposed to oral bacteria secrete EVs; the event leads to inflammation and tissue destruction by modulating fibroblasts [11]. The periodontal ligament fibroblasts treated with *Pg* LPS also release EVs that are incorporated into osteoblasts and inhibit their differentiation [12]. These findings suggest that EVs released from periodontal tissues may play an important role in periodontal diseases.

EVs are also known to deliver bacterial virulence factors from the primary infectious site to distant organs. Gastric epithelial cells infected with *Helicobacter pylori* release EVs that contain the bacterial virulence factor cytotoxin-associated gene A (CagA) [13]. CagA-rich EVs are taken up into the blood circulation and reach distant organs and affect the development of extra-gastric diseases such as diabetes mellitus and Alzheimer's disease [14]. These findings suggest that EVs may provoke mechanisms by

85 which bacterial infection affects systemic diseases. However, the role of EVs in periodontal medicine
86 remains unclear.

87 In this study, we tested the hypothesis that EVs released from periodontal bacteria-infected cells are
88 implicated in the development of periodontal medicine. We focused on macrophages as donor cells that
89 release EVs because macrophages play key roles in periodontal diseases by protecting the periodontal
90 tissue from infection via phagocytosis [15] and by destroying it via pro-inflammatory cytokine release
91 [16]. This study aimed to investigate whether EVs derived from *Pg*-infected (*Pg*-inf) macrophages
92 reach distant organs in mice and could affect the pathophysiological status.

93

2. Materials and Methods

2. 1. Bacterial cultures

SNAP-*Pg* (S-*Pg*) was constructed by transforming the *SNAP26b* gene into *P. gingivalis* ATCC33277 as described previously[1]. S-*Pg* or *P. gingivalis* ATCC33277 were cultured in Brain Heart Infusion medium (BD Bioscience, Franklin Lakes, NJ) containing 0.5% yeast extract (BD Bioscience), 10 μg/mL hemin (Wako Chemicals, Osaka, Japan), 1 μg/mL 2-methyl-1,4-naphthoquinone (vitamin K3) (Tokyokasei, Tokyo, Japan), and 5 μg/mL tetracycline in an anaerobic jar at 37°C. *F. nucleatum* (*Fn*) was cultured in Brain Heart Infusion medium with 5 μg/mL hemin and 1 μg/mL vitamin K3 in an anaerobic jar at 37°C.

2. 2. Cell culture

The human monocytic cell line THP-1 was seeded at a concentration of 30,000 cells/mL and cultured in RPMI 1640 or DMEM medium supplemented with 10% FBS at 37°C under a humidified atmosphere of 5% CO_2.

Human alveolar epithelial-like type-II cells A549 were suspended in DMEM supplemented with 10% FBS at a concentration of 10,000 cells/mL, and cultured for 3 days at 37°C under a humidified atmosphere of 5% CO_2.

2. 3. Bacterial infection

At 24 h after seeding, THP-1 cells were differentiated into macrophages by treatment with 100 nM phorbor myristate acetate (PMA) for 48 h. THP-1 cells were treated with *Pg* (MOI = 100) for 4 h in RPMI 1640 medium with 2% FBS, and then the unincorporated *Pg* was washed away with PBS. The *Pg*-infected THP-1 cells were incubated for 48 h in RPMI 1640 medium with 2% exosome-free FBS, and EVs released into the culture medium were collected and isolated.

2. 4. Detection of fluorescent-labeled Pg

Pg was incubated with CytoTell UltraGreen (AAT Bioquest) for 10 min at 37 °C and then treated with host cells at a concentration of 100 MOI for the indicated periods. The cells were fixed with 4% formalin for 30 min and then permeabilized with 0.1% Triton X-100 in PBS for 2 min on ice, followed by Hoechst 33342 for 30 min. The samples were observed using a Nikon A1 laser fluorescence confocal microscope (A1 R HD25, Nikon). Images were acquired using NIS-Elements software (Nikon).

2. 5. Colony-forming unit (CFU) determination

THP-1 cells were treated with *Pg* for 4 h and then treated with antibiotics (200 μg/mL metronidazole and 300 μg/mL gentamicin) for 60 min to remove *Pg* from the cell surface. The cells were lysed by adding 200 μL of H_2O, and the extract was spread on blood agar using a spiral plater (EDDY-Jet, IUL Instruments). Blood agar was incubated for 5 days in an anaerobic jar at 37 °C. Colony counting and CFU determination were performed according to the manufacturer's instructions

2. 6. EVs isolation

EVs were isolated from the culture medium by polymer-based precipitation methods as previously described [17]. Briefly, the culture medium was centrifuged at 2,000 × *g* for 30 min at 4 °C to remove cell debris. The supernatant was centrifuged at 10,000 × *g* for 30 min at 4 °C, filtered with a 0.2-μm syringe filter, and concentrated using an Ultra-15 Centrifugal Filter Device for a nominal molecular weight limit (NMWL) of 100,000 (Amicon). The concentrate was mixed with Total Exosome Isolation Reagent (Thermo Fisher Scientific) and incubated for 16 h at 4 °C. The samples were then centrifuged at 10,000 × *g* for 60 min at 4 °C. The EV fractions were eluted with PBS. The diameter of the EVs was measured using a Zetasizer Nano ZSP (Malvern Panalytical). The morphology of the EVs was observed using transmission electron microscopy (TEM), as described previously [18].

2. 7. Animals

BALB/cAJc1 mice (female, 40 weeks old) were purchased from Japan CLEA (Tokyo, Japan) and fed a high-fat diet (Quick Fat, 15.3% fat, 424.5 kcal/100 g; Japan CLEA). Mice were randomly grouped to the control or experimental group, respectively, and housed under specific-pathogen free conditions. The mice were maintained and handled according to the Fundamental Guidelines for Proper Conduct of Animal Experiment and Related Activities in Academic Research Institutions (the Ministry of Education, Culture, Sports, Science and Technology, Japan, 2006). All animal experiments were approved by the Ethics Committee of Animal Care and Experimentation of Tokushima University (approval number T29-3) and conform to the ARRIVE (Animal Research: Reporting of In Vivo Experiments) guidelines.

2. 8. In vivo imaging

EVs (15 μg of total protein) were incubated with 5 μM Cy7 Mono NHS Ester (GE Healthcare) for 90 min at 37 °C. The unincorporated dye was removed using exosome spin columns (Thermo Fisher Scientific). Cy7-labeled EVs were injected intraperitoneally into mice (n = 3 in each group). At 2 h post-injection, Cy7 fluorescence was analyzed in organs using an IVIS Spectrum imaging system (Caliper Life Sciences).

To monitor inflammation by targeting MPO activity, the XenoLight RediJect Inflammation Probe (Perkin Elmer) was intraperitoneally injected into mice which were intraperitoneally injected with EVs (5 μg of total protein) or PBS for 12 weeks at 3-day intervals (3 mice in each group) at a dose of 200 mg/kg. At 10 min post-injection, the organs were removed and luminescence signals were detected using an IVIS Spectrum imaging system.

2. 9. Histological analysis and Immunohistochemistry

The mice were intraperitoneally injected with EVs (5 μg of total protein) or PBS for 4 h (acute phase, 4 mice in each group) or 12 weeks at 3-day intervals (for a prolonged effect, 5 mice in each group). After the indicated periods, mouse lung tissues were removed and fixed in 4% paraformaldehyde phosphate buffer solution (Nacalai Tesque) for 48 h at 4 °C and embedded in paraffin wax. Serial sections (4 μm thick) were prepared and stained with hematoxylin and eosin (H&E) or Masson trichrome staining.

The antigens were retrieved by heating the sections in 0.1 M buffer. The sections were incubated in 0.3% H_2O_2 in methanol for 30 min and then treated with 4% BSA in PBS for 60 min. After incubation with anti-fibrinogen antibody (1:500, GeneTex) or normal rabbit IgG for 16 h at 4 °C, immunoreactive sites were identified using the SignalStain Boost Detection reagent (Cell Signaling Technology). To detect neutrophils, the sections were incubated with an antibody against neutrophil elastase (1:200; BIOSS) or normal rabbit IgG for 16 h. The sections were incubated with Alexa Fluor 594-conjugated secondary antibody (1:500; Invitrogen) for 45 min at RT and then treated with Hoechst 33342 for 30 min. The sections were observed using a BZ-X800 (Keyence) or an inverted fluorescence microscope (ECLIPSE Ti-U, Nikon).

2. 10. Immunocytochemistry

A549 cells were fixed with 4% formalin for 30 min and then permeabilized with 0.1% Triton X-100 in PBS for 2 min on ice. After blocking with 4% BSA in PBS for 45 min, the cells were incubated with anti-NF-κB κ p65 antibody (F-6, Santa Cruz Biotechnology, sc-8008) or histone H3 (Medical & Biological Laboratories) normal mouse IgG overnight at 4°C, followed by Alexa Fluor 566-conjugated anti-rabbit IgG for 1 h. The cells were then treated with Hoechst 33342 for 30 min for nuclear staining. The samples were mounted and observed using a ECLIPSE Ti-U.

2. 11. SDS-PAGE and western blot analysis

193 The cells were scraped into lysis buffer, separated by SDS-PAGE, and transferred to PVDF membranes
194 (Immobilon-P, Millipore). The primary antibodies used were SNAP-tag rabbit polyclonal antibody
195 (1:1000, P9310S, New England Biolabs), histone H3 (1:1000, MABI0301, Medical & Biological
196 Laboratories), CD11b/ITGAM (D6X1N) (1:1000, #49420, Cell Signaling), CD9 (D801A) (1:1000,
197 #413174, Cell Signaling), and β-actin (1:1000, 60008-1, Proteintech), IκB-alpha (1:1000, #9242, Cell
198 Signaling Technology), phospho p65 (Ser 536) (1:1000, #3033, Cell Signaling Technology) and p65
199 (1:1000, sc-372, Santa Cruz Biotechnology). The membranes were washed with TBS-T for 30 min at
200 RT and incubated with anti-mouse IgG and HRP-linked antibody (1:10000, #7076, Cell Signaling
201 Technology) for 45 min at RT, and then the signals were detected using Western BLoT
202 Chemiluminescence HRP Substrate (Takara).
203
204 *2. 12. Protein identification by mass spectrometry*
205 The digested protein fraction was subjected to mass spectrometric analysis, as described previously[18].
206 Briefly, the sample was injected into a nano-LC system (Waters, Milford, MA, USA) and separated
207 with a gradient of 5–50% solvent B for 45 min at a flow rate of 200 nL/min. The peptides were
208 continuously analyzed using a Q-Tof Ultima API (Waters), and the MS scan was performed. The MS
209 and MS/MS data obtained were searched for human origin and analyzed using the Swiss-Prot database
210 and the MASCOT server program (version 2.0.05; Matrix Science Ltd). Proteins were identified by
211 using only one peptide with a score higher than 40. The search results showed a false discovery rate of
212 < 5%.
213
214 *2. 13. RNA isolation and real-time PCR*
215 The mice were intraperitoneally injected with EVs (5 μg of total protein) or PBS for 12 weeks at 3-day
216 intervals (BALB/cAJc1 mice, female, 30 weeks old 4 mice in each group). After the indicated periods,
217 mouse lung tissues were removed and homogenized in ISOGEN (Nippon Gene) and total RNA was
218 isolated according to the manufacture's protocol. The cDNA was synthesized by using Prime

Script™ RT reagent kit (Takara Bio, Kyoto, Japan). Real-time PCR was performed with the 7300 Real-Time PCR system (Applied Biosystems, Carlsbad, CA, USA) using SYBR Premix Ex Taq™ (Takara Bio). The sequences of primers were as follows: mouse GAPDH (NM_001001303): forward, 5'-TGTGTCCGTCGTGGATCTGA-3', reverse, 5'-TTGCTGTTGAAGTCGCAGGAG-3'; mouse TNF-α (NM_013693): forward, 5'-TATGGCCCAGACCCTCACA-3', reverse, 5'-GGAGTAGACAAGGTACAACCCATC-3'; mouse IL-6 (NM_031168): forward, 5'-CCACTTCACAAGTCCGAGGATTA-3', reverse, 5'-GCAAGTGCATCATCGTTGTTCATAC-3'.

2. 14. Lactate dehydrogenase (LDH) release

THP-1 cells were infected with *Pg* or *Fn* for 4 h, and removed unincorporated bacteria by washing with PBS. Then, THP-1 cells were cultured for further 48 h, and aliquots of culture medium were collected to measure extracellular LDH activity using LDH cytotoxity assay kits (cayman Chemical Company, cat no 10008882) according to the manufacture's protocol.

2. 15. Propidium iodide (PI) and Hoechst 33342 staining

THP-1 cells were infected with PG or Fn and cultured for 48 h as descrived above. Then, the cells were incubated with 1 μg/mL of PI and Hoechst 33342 for 15min, and examined under an ECLIPSE Ti-U microscope and NIS-Elements software (Nikon).

2. 16. Statistical analysis

Statistical analyses were performed using the Statcel2 software. The normal distribution of the data was first examined using the chi-squared test. The variables that had a normal distribution were analyzed using the Student's *t*-test. *In vitro* experiments were performed independently at least 3 times and all data are expressed as the mean ± standard deviation (SD). *In vivo* studies (*in vivo* imaging, histological

243 analysis and Immunohistochemistry) were performed independently 3 times and the typical results were
244 shown.
245

3. Results

3. 1. Pg-inf THP-1 cells released EVs

The EVs isolation schedule is shown in Figure 1A. THP-1 cells were treated with SNAP26b tagged protein-expressing *Pg* (S-*Pg*) to trace *Pg* translocation inside the cells. SNAP26b protein was detected in S-*Pg*-treated THP-1 cells at 2 h and after (Fig. 1B). The fluorescent-labeled *Pg* ATCC33277 (*Pg*) was observed mostly in the cytoplasm of THP-1 cells at the end of the *Pg* treatment for 4 h and remained inside the THP-1 cells at 24 - 48 h post-treatment (Fig. 1C). At the end of *Pg* treatment for 4 h, *Pg* within THP-1 cells formed colonies on blood agar (Fig. 1D). At 24 and 48 h after *Pg* treatment, colony formation was still detected on blood agar, whereas its CFU decreased. We also confirmed that *Pg*-treated THP-1 cells did not show typical cell death features such as cell shedding, propidium ioide (PI)-positive cells, and lactate dehydrogenase (LDH) leakage (Supplementary Figure 1). These results suggested that *Pg* invaded THP-1 cells and survived for at least 48 h without inducing host cell death. Since infection is identified by bacterial invasion into the host cells and their survival in the intracellular location [19], THP-1 cells were considered to be infected with *Pg* in this study.

Next, we purified EVs from a culture medium of THP-1 cells infected with or without *Pg* and analyzed them using TEM. Round-shaped EVs were found in the EV fraction isolated from the culture media of THP-1 cells. There were no differences in EV shape (Fig. 1E) and size (Supplementary Figure 2) between the EVs derived from non-infected (No-inf EVs) and *Pg*-infected THP-1 cells (*Pg*-inf EVs).

3. 2. EVs of Pg-inf THP-1 cells included histone proteins

Pg-inf EVs or No-inf EVs were subjected to SDS-PAGE, and major EV protein bands on the silver-stained gel were observed. We found that low-molecular-weight proteins were specifically present in *Pg*-inf EVs (Fig. 2A, lane 2). The bands corresponding to these low-molecular-weight proteins were identified as multiple core histones, including histone H2A, H2B, H3, and H4 by Nano-LC-MS/MS (Supplementary Table 1). In *Pg-infected* THP-1 cells, leaking of histone H3 proteins from the nucleus was observed (Fig. 2B). Western blotting revealed that histone H3 proteins were detected in the *Pg*-inf

EVs, but not in the No-inf EVs (Fig. 2C). The significant increase in histone H3 proteins in the *Pg*-inf EVs was also confirmed using ELISA (Fig. 2D).

Pg internalizes in cells via endocytosis, followed by the accumulation of actin fibers and microtubules [20]. To block *Pg* invasion, THP-1 cells were pretreated with cytochalasin D that inhibits actin polymerization. The colony formation of *Pg* decreased significantly in cytochalasin D-pretreated THP-1 cells at 4 h post-*Pg* infection, indicating that cytochalasin blocked *Pg* from invading THP-1 cells (Fig. 2E). The blocking of *Pg* invasion by cytochalasin D decreased the amount of histone H3 in *Pg*-inf EVs at 48 h post-*Pg* infection (Fig. 2F, lane 3), suggesting that the internalization of *Pg* was important for the leakage and packaging of histone H3 into EVs.

3. 3. EVs of THP-1 cells translocated to multiple organs in mice

Pg-inf EVs and No-inf EVs were labeled using Cy7 fluorescent dye and injected intraperitoneally into mice. As a negative control, PBS was using the same procedure and injected into the abdominal cavity of the mice. At 2 h post-injection, organs were extracted, and the distribution of the Cy7-labeled EVs was analyzed using an IVIS Spectrum imaging system. In mice injected with *Pg*-inf EVs and No-inf EVs, but not in PBS-injected mice, Cy7-fluorescent signals were detected in the liver, lungs, and kidneys, revealing that EVs derived from THP-1 cells could translocate to distant organs independent of *Pg* infection (Fig. 3A).

Since *Pg* can invade a variety of host cells and remain viable [21, 22], we confirmed whether other non-phagocytic cells infected with *Pg* release EVs that have the same properties as THP-1 cells. *Pg* resided in non-phagocytic cells, such as mouse osteoblastic MC3T3-E1 cells, human gingival epithelial TR146 cells, and human hepatocyte HepG2 at 4 h post-infection (Supplementary Figure 3A). These *Pg*-treated non-phagocytic cells released EVs of different sizes 48 h after treatment (Supplementary Figure 3B). These EVs were labeled with Cy7 and injected into the abdominal cavity of the mice. Fluorescence was detected only in the livers of mice injected with EVs from *Pg*-infected non-

297 phagocytic cells (Fig. 3B), suggesting that EVs of THP-1 cells may have special characteristics to
298 translocate to multiple organs.
299
300 *3. 4. Pg-inf EVs induced pulmonary injury in mice*
301 *Pg*-inf EVs or No-inf EVs were intraperitoneally injected, and the lungs were prepared for
302 histochemical examination 4 h after injection. Mice injected with *Pg*-inf EVs showed widespread edema
303 (Fig. 4A; b, and d). In these mice, pulmonary interstitial tissue was thickened, and many erythrocytes
304 (Fig 4A; d) and fibrinogen deposition (Fig 4A; e) and infiltration of neutrophils were observed (Fig 4B).
305 These pathological changes were not detected in the lungs of PBS-injected control mice or No-inf EV-
306 injected mice, suggesting that the injection of *Pg*-inf EVs immediately leads to the acute phase of lung
307 injury, including edema, vascular congestion, and neutrophil infiltration.
308 Furthermore, we analyzed whether prolonged administration of EVs for 12 weeks induced
309 pathological changes in the lungs. Inflammation in organs was monitored using the XenoLight RediJect
310 Inflammation Probe. In mice administered *Pg*-inf EVs, but not No-inf EVs or PBS, luminescence
311 signals were detected in the lungs and spleen (Fig. 4C). The mRNA expression of inflammatory
312 mediators significantly increased in mice administered *Pg*-inf EVs (Fig. 4D). Collagen deposition
313 around small vessels markedly increased in *Pg*-inf EV-injected mice (Fig. 4E). In *Pg*-inf EV-injected
314 mice, collagen deposition reached the pulmonary interstitial tissue, and the alveolus structures were
315 compromised (Fig. 4E; b, d). These results showed that prolonged administration of *Pg*-inf EVs induced
316 pulmonary inflammation, resulting in collagen deposition in the interstitial tissue and alveolar
317 destruction.
318
319 *3. 5. Histone H3 in Pg-inf EVs increased inflammatory cytokines via the NF-κB pathway in A549 cells*
320 We further investigated the mechanisms by which *Pg*-inf EVs regulate inflammation by using alveolar
321 epithelial A549 cells. *Pg*-inf EVs increased the mRNA expression of IL-6 and TNF-α in a dose-
322 dependent manner (Fig. 5A). These cytokine-induced effects were not observed in the No-inf EV-

323 treated A549 cells. Pretreatment with BAY, an inhibitor of nuclear factor κB (NF-B), attenuated the
324 mRNA expression of IL-6 and TNF-α increased by *Pg*-inf EVs (Fig. 5B). The *Pg*-inf EVs induced the
325 degradation of IκB, leading to phosphorylation of p65 in A549 cells (Fig. 5C). The phosphorylated p65
326 translocated to the nucleus 60 min after *Pg*-inf EV treatment (Fig. 5D). These observations suggested
327 that *Pg*-inf EVs, but not No-inf EVs, induce inflammation via the NF-κB pathway.
328 Furthermore, recombinant histone H3 increased IL-6 and TNF-α mRNA expression
329 (Supplementary Figure 4A), and inhibition of the NF-κB pathway by BAY attenuated the effects of
330 recombinant histone H3 on the expression of these cytokines (Supplementary Figure 4B). The digestion
331 of histone H3 in *Pg*-inf EVs using trypsin did not induce phosphorylation of p65 (Fig. 5E), resulting in
332 failed IL-6 and TNF-α mRNA induction (Fig. 5F). These findings suggest that histone H3 in *Pg*-inf
333 EVs may contribute to lung inflammation by activating the NF-κB pathway.
334

4. Discussion

The prevalence of periodontal medicine is also dependent on various factors other than periodontitis caused by periodontal bacteria. Among these factors, aging and a high-fat diet are considered important. For example, in a mouse model of Alzheimer's disease, *Pg* or *Pg* lipopolysaccharide (LPS) caused cognitive impairment via an increase in neuroinflammation in middle-aged mice, but not in young adult mice [23, 24]. Oral administration of *Pg* or *Pg* LPS accelerated the development of periodontal medicine such as atherosclerosis [25] and diabetes mellitus [26] in mice fed a high-fat diet. Therefore, in this study, we used middle-aged mice (40 weeks old), and fed them a high-fat diet to investigate the effect of EVs on their pathophysiological status.

THP-1 constantly secreted EVs that translocate to the lungs, liver, and kidneys, independent of *Pg*-infection. The Cy7-labeled EVs of THP-1 cells administrated to mice tail vein or orbital venous plexus accumulated in the lungs (data not shown), suggesting that EVs of THP-1 cells can be stabilized in the body fluids and reach the lungs through the systemic circulation. Since EVs from non-phagocytic cells did not enter the lungs and kidneys (Fig. 3B), macrophages seemed to have the potential to produce EVs that translocate to multiple organs. In the present study, we injected EVs into the abdomen of mice because intraperitoneal injection appeared to facilitate EV uptake in the systemic circulation [27]. To verify whether periodontal infection affects systemic diseases, it might be more useful to inject EVs into the oral cavity. However, experimental models directly uptake EVs into the circulation via periodontal tissue or orally in mice. Therefore, the factors generated during periodontal infection, such as outer membrane vesicles (OMVs), EVs, and bacterial components, are often injected via routes other than oral administration. For example, intracardiac injection of *Aggregatibacter actinomycetemcomitans* OMVs in mice led to increased TNF-α expression in the brain, showing that the infection was delievred to the brain [28]. The injection of *Pg* OMV into the common cardinal vein induced vascular diseases in zebrafish [29], and lipopolysaccharides of *Pg* injected into the abdominal cavity impaired spatial learning and memory with neuroinflammation in mice [30].To gain further

360 understanding of the pathogenesis of periodontal medicines, it is necessary to establish experimental
361 models that directly uptake EVs into the circulation via periodontal tissue or oral cavity in mice.
362 The mechanisms by which EVs derived from THP1 cells translocate to multiple organs have not
363 been clarified in this study. EVs display different integrin proteins on their surface that promote
364 adhesion to cells at specific target sites in organs [31]. For example, EVs displaying integrin $\alpha_6\beta_4$ fuse
365 preferentially with laminin-expressing fibroblasts and epithelial cells in the lung [32]. Therefore, it is
366 worth analyzing the differences in the integrin profiles of EVs between macrophages and non-
367 macrophages in the future.
368 The translocation of *Pg*-inf EVs to the lungs immediately induced pulmonary edema, hemorrhage,
369 thrombosis, and neutrophil infiltration (Fig. 4A, B). Prolonged administration of *Pg*-inf EVs resulted in
370 inflammation (Fig. 4C, D) and alveolar destruction (Fig. 4E). The pathological changes induced by *Pg*-
371 inf EVs are consistent with those of lung injury commonly observed in many types of pulmonary
372 diseases, such as fibrosis [33] and chronic obstructive pulmonary disease (COPD) [34]. A recent study
373 showed that periodontitis severity is positively associated with the risk of COPD [35], and the alteration
374 of neutrophil functions caused by periodontitis may result in tissue damage in COPD [36]. Our results
375 also raised the possibility that EVs produced by *Pg*-infected macrophages might be implicated in the
376 progression of pulmonary injury.
377 We speculated that histones were responsible for *Pg*-inf EV-induced pulmonary injury because
378 histone proteins were specifically sorted into EVs by *Pg* infection (Fig. 2A, Supplementary Table 1).
379 Indeed, both *Pg*-inf Evs and recombinant histone H3 could induce inflammation by activating NF-κB
380 signaling in A549 cells, and digestion of histone H3 in *Pg*-inf Evs using trypsin prevented NF-κB
381 activation following *Pg*-inf EV treatment. Histones are intra-nuclear proteins present in eukaryotic cells
382 that are highly conserved across species and provide normal chromatin structures. Histones are also
383 released into the extracellular space under pathological conditions and elicit pro-inflammatory and
384 cytotoxic effects on host cells [37]. Reports on extracellular histones contributing to lung injury [38,
385 39] and COPD [40] support our results. However, it should be mentioned that the role of histone H3 in

EVs is only based on *in vitro* studies conducted using A549 cells (Fig. 5); this role was not explored *in vivo*. Trypsin, which is a serine protease that indiscriminately digests any protein, was used to digest histone H3 in EVs in this study. It is possible that EVs contain various types of cargo that promote lung injury other than histones. To clarify the roles of histone H3 in EVs, a neutralizing antibody for Histone H3 should be used to show that EVs promote NF-κB activation in a histone H3 dependent manner in mice.

Extracellular histones are released from dying cells during necrosis or neutrophil NET, a type of cell death dependent on the formation of extracellular traps (NETs) [41]. It has been reported that macrophages also produce similar extracellular traps in response to various microorganisms [42]. However, infection with *Pg* caused less host cell death, and no morphological changes indicating NET formation were observed in the *Pg*-infected macrophages (Supplementary Figure 1). In contrast, the inhibition of actin polymerization by cytochalasin D resulted in the attenuation of *Pg*-induced histone H3 packaging into EVs (Fig. 2F). These observations suggest that the internalization of *Pg* into macrophages may play an important role in the release of histones from the nucleus in macrophages. However, the possibility that cytochalasin D reduces phagocytosis of *Pg* or EV production should be clarified. Based on the fact that *Pg* can survive inside macrophages during EV production (Fig. 1D), further studies are needed to investigate whether live *Pg* inside the cells could approach the nucleus and affect the release of histones.

Our results suggest that EVs released by *Pg*-infected macrophages may translocate to the lungs and modulate pulmonary injury. Moreover, we cannot rule out the possibility that administering EVs from human THP-1 cells into mice may result in an MHC-II-mediated immune response. Because EVs of uninfected THP-1 cells also localize to multiple organs (Fig. 3A), it is possible that the observations are a consequence of the immune response. To verify this possibility, these findings should be further confirmed using mouse primary monocytes or bone marrow cell-derived macrophages.

In conclusion, our findings raise the possibility that periodontal pathogen-infected macrophages may produce cytotoxic EVs that induce pulmonary injury, and suggest a potential mechanism by which

412 periodontal diseases contribute to the progression of periodontal medicine. At present, professional oral
413 health care aimed at reducing oral bacteria is limited to elderly persons and patients with swallowing
414 difficulties because aspiration of bacteria into the respiratory tract has been considered to cause
415 pneumonia. However, the present results suggest that oral hygiene may affect lung inflammation via
416 EVs without bacterial aspiration and that professional oral care may be important for maintaining
417 general health in a wider population.
418

Acknowledgments

We thank the Support Center for Advanced Medical Sciences (Institute of Health Biosciences, University of Tokushima Graduate School) for the LC-MS/MS analyses and technical support.

This study was supported by a Grant-in-Aid for Scientific Research from the Ministry of Education, Science, Sports, and Culture of Japan (20K21714, Kaya Yoshida; 19H04051, HO), SHISEIDO Female Researcher Science Grant (Kaya Yoshida).

The authors declare no competing financial interests.

Author contributions

Kaya Yoshida, H. Okamura, and K. Ozaki conceived and supervised the project. Kaya Yoshida, M. Seyama, and Kayo Yoshida performed the majority of the experiments. N. Fujiwara performed a colony formation assay. Ono and Sasaki analyzed EVs. H. Kawai and H. Nagatsuka contributed to the pathological diagnosis by H&E staining. J. Guo and Y. Yu designed the figures. Kaya Yoshida and H. Okamura wrote the manuscript with input from all authors. Y. Weng, Z. Wang, Y. Fukuhara, and M. Ikegame edited the manuscript.

References

[1] M. Ishikawa, K. Yoshida, H. Okamura, K. Ochiai, H. Takamura, N. Fujiwara, K. Ozaki, Oral Porphyromonas gingivalis translocates to the liver and regulates hepatic glycogen synthesis through the Akt/GSK-3beta signaling pathway, Biochim. Biophys. Acta 1832(12) (2013) 2035-43.

[2] H. Takamura, K. Yoshida, H. Okamura, N. Fujiwara, K. Ozaki, Porphyromonas gingivalis attenuates the insulin-induced phosphorylation and translocation of forkhead box protein O1 in human hepatocytes, Arch. Oral Biol. 69 (2016) 19-24.

[3] I. Olsen, S.K. Singhrao, J. Potempa, Citrullination as a plausible link to periodontitis, rheumatoid arthritis, atherosclerosis and Alzheimer's disease, J Oral Microbiol 10(1) (2018) 1487742.

[4] S.S. Dominy, C. Lynch, F. Ermini, M. Benedyk, A. Marczyk, A. Konradi, M. Nguyen, U. Haditsch, D. Raha, C. Griffin, L.J. Holsinger, S. Arastu-Kapur, S. Kaba, A. Lee, M.I. Ryder, B. Potempa, P. Mydel, A. Hellvard, K. Adamowicz, H. Hasturk, G.D. Walker, E.C. Reynolds, R.L.M. Faull, M.A. Curtis, M. Dragunow, J. Potempa, in Alzheimer's disease brains: Evidence for disease causation and treatment with small-molecule inhibitors, Sci Adv 5(1) (2019) eaau3333.

[5] J.D. Beck, P.N. Papapanou, K.H. Philips, S. Offenbacher, Periodontal Medicine: 100 Years of Progress, J. Dent. Res. 98(10) (2019) 1053-1062.

[6] M. Mathieu, L. Martin-Jaular, G. Lavieu, C. Théry, Specificities of secretion and uptake of exosomes and other extracellular vesicles for cell-to-cell communication, Nat. Cell Biol. 21(1) (2019) 9-17.

[7] M. Pathan, P. Fonseka, S.V. Chitti, T. Kang, R. Sanwlani, J. Van Deun, A. Hendrix, S. Mathivanan, Vesiclepedia 2019: a compendium of RNA, proteins, lipids and metabolites in extracellular vesicles, Nucleic Acids Res. 47(D1) (2019) D516-d519.

[8] R. Kalluri, V.S. LeBleu, The biology, function, and biomedical applications of exosomes, Science 367(6478) (2020).

[9] M. Yáñez-Mó, P.R. Siljander, Z. Andreu, A.B. Zavec, F.E. Borràs, E.I. Buzas, K. Buzas, E. Casal, F. Cappello, J. Carvalho, E. Colás, A. Cordeiro-da Silva, S. Fais, J.M. Falcon-Perez, I.M. Ghobrial, B. Giebel, M. Gimona, M. Graner, I. Gursel, M. Gursel, N.H. Heegaard, A. Hendrix, P. Kierulf, K. Kokubun, M. Kosanovic, V. Kralj-Iglic, E.M. Krämer-Albers, S. Laitinen, C. Lässer, T. Lener, E. Ligeti, A. Linē, G. Lipps, A. Llorente, J. Lötvall, M. Manček-Keber, A. Marcilla, M. Mittelbrunn, I. Nazarenko, E.N. Nolte-'t Hoen, T.A. Nyman, L. O'Driscoll, M. Olivan, C. Oliveira, É. Pállinger, H.A. Del Portillo, J. Reventós, M. Rigau, E. Rohde, M. Sammar, F. Sánchez-Madrid, N. Santarém, K. Schallmoser, M.S. Ostenfeld, W. Stoorvogel, R. Stukelj, S.G. Van der Grein, M.H. Vasconcelos, M.H. Wauben, O. De Wever,

Biological properties of extracellular vesicles and their physiological functions, J Extracell Vesicles 4 (2015) 27066.
[10] A. Chaparro Padilla, L. Weber Aracena, O. Realini Fuentes, D. Albers Busquetts, M. Hernández Ríos, V. Ramírez Lobos, A. Pascual La Rocca, J. Nart Molina, V. Beltrán Varas, S. Acuña-Gallardo, A. Sanz Ruiz, Molecular signatures of extracellular vesicles in oral fluids of periodontitis patients, Oral Dis. (2020).
[11] J. Bi, L. Koivisto, G. Owen, P. Huang, Z. Wang, Y. Shen, L. Bi, A. Rokka, M. Haapasalo, J. Heino, L. Häkkinen, H.S. Larjava, Epithelial Microvesicles Promote an Inflammatory Phenotype in Fibroblasts, J. Dent. Res. 95(6) (2016) 680-8.
[12] M. Zhao, W. Dai, H. Wang, C. Xue, J. Feng, Y. He, P. Wang, S. Li, D. Bai, R. Shu, Periodontal ligament fibroblasts regulate osteoblasts by exosome secretion induced by inflammatory stimuli, Arch. Oral Biol. 105 (2019) 27-34.
[13] A. Shimoda, K. Ueda, S. Nishiumi, N. Murata-Kamiya, S.A. Mukai, S. Sawada, T. Azuma, M. Hatakeyama, K. Akiyoshi, Exosomes as nanocarriers for systemic delivery of the Helicobacter pylori virulence factor CagA, Sci. Rep. 6 (2016) 18346.
[14] E. Goni, F. Franceschi, Helicobacter pylori and extragastric diseases, Helicobacter 21 Suppl 1 (2016) 45-8.
[15] T. Berglundh, M. Donati, Aspects of adaptive host response in periodontitis, J Clin Periodontol 32 Suppl 6 (2005) 87-107.
[16] J. Yang, Y. Zhu, D. Duan, P. Wang, Y. Xin, L. Bai, Y. Liu, Y. Xu, Enhanced activity of macrophage M1/M2 phenotypes in periodontitis, Arch Oral Biol 96 (2018) 234-242.
[17] K. Ono, T. Eguchi, C. Sogawa, S.K. Calderwood, J. Futagawa, T. Kasai, M. Seno, K. Okamoto, A. Sasaki, K.I. Kozaki, HSP-enriched properties of extracellular vesicles involve survival of metastatic oral cancer cells, J. Cell. Biochem. 119(9) (2018) 7350-7362.
[18] M. Seyama, K. Yoshida, N. Fujiwara, K. Ono, T. Eguchi, H. Kawai, J. Guo, Y. Weng, Y. Haoze, K. Uchibe, M. Ikegame, A. Sasaki, H. Nagatsuka, K. Okamoto, H. Okamura, K. Ozaki, Outer membrane vesicles of Porphyromonas gingivalis attenuate insulin sensitivity by delivering gingipains to the liver, Biochim Biophys Acta Mol Basis Dis 1866(6) (2020) 165731.
[19] G. Rollin, X. Tan, F. Tros, M. Dupuis, X. Nassif, A. Charbit, M. Coureuil, Intracellular Survival of, Front Microbiol 8 (2017) 1354.
[20] A. Amano, N. Furuta, K. Tsuda, Host membrane trafficking for conveyance of intracellular oral pathogens, Periodontol 2000 52(1) (2010) 84-93.
[21] O. Yilmaz, P. Verbeke, R.J. Lamont, D.M. Ojcius, Intercellular spreading of Porphyromonas gingivalis infection in primary gingival epithelial cells, Infect Immun 74(1) (2006) 703-10.

[22] K. Yoshida, H. Okamura, Y. Hiroshima, K. Abe, J.I. Kido, Y. Shinohara, K. Ozaki, PKR induces the expression of NLRP3 by regulating the NF-κB pathway in Porphyromonas gingivalis-infected osteoblasts, Exp. Cell Res. 354(1) (2017) 57-64.
[23] Y. Ding, J. Ren, H. Yu, W. Yu, Y. Zhou, Porphyromonas gingivalis, a periodontitis causing bacterium, induces memory impairment and age-dependent neuroinflammation in mice, Immun. Ageing 15 (2018) 6.
[24] K. Hayashi, Y. Hasegawa, Y. Takemoto, C. Cao, H. Takeya, Y. Komohara, A. Mukasa, S. Kim-Mitsuyama, Continuous intracerebroventricular injection of Porphyromonas gingivalis lipopolysaccharide induces systemic organ dysfunction in a mouse model of Alzheimer's disease, Exp. Gerontol. 120 (2019) 1-5.
[25] J.S. Suh, S. Kim, K.I. Boström, C.Y. Wang, R.H. Kim, N.H. Park, Periodontitis-induced systemic inflammation exacerbates atherosclerosis partly via endothelial-mesenchymal transition in mice, Int J Oral Sci 11(3) (2019) 21.
[26] K. Watanabe, S. Katagiri, H. Takahashi, N. Sasaki, S. Maekawa, R. Komazaki, M. Hatasa, Y. Kitajima, Y. Maruyama, T. Shiba, K. Komatsu, Y. Ohsugi, K. Tanaka, A. Matsuzawa, T. Hirota, H. Tohara, Y. Eguchi, K. Anzai, A. Hattori, T. Iwata, Porphyromonas gingivalis impairs glucose uptake in skeletal muscle associated with altering gut microbiota, FASEB J. 35(2) (2021) e21171.
[27] S.C. Jang, S.R. Kim, Y.J. Yoon, K.S. Park, J.H. Kim, J. Lee, O.Y. Kim, E.J. Choi, D.K. Kim, D.S. Choi, Y.K. Kim, J. Park, D. Di Vizio, Y.S. Gho, In vivo kinetic biodistribution of nano-sized outer membrane vesicles derived from bacteria, Small 11(4) (2015) 456-61.
[28] E.C. Han, S.Y. Choi, Y. Lee, J.W. Park, S.H. Hong, H.J. Lee, Extracellular RNAs in periodontopathogenic outer membrane vesicles promote TNF-α production in human macrophages and cross the blood-brain barrier in mice, FASEB J. 33(12) (2019) 13412-13422.
[29] C. Farrugia, G.P. Stafford, C. Murdoch, Porphyromonas gingivalis Outer Membrane Vesicles Increase Vascular Permeability, J. Dent. Res. 99(13) (2020) 1494-1501.
[30] J. Zhang, C. Yu, X. Zhang, H. Chen, J. Dong, W. Lu, Z. Song, W. Zhou, Porphyromonas gingivalis lipopolysaccharide induces cognitive dysfunction, mediated by neuronal inflammation via activation of the TLR4 signaling pathway in C57BL/6 mice, J. Neuroinflammation 15(1) (2018) 37.
[31] H. Peinado, H. Zhang, I.R. Matei, B. Costa-Silva, A. Hoshino, G. Rodrigues, B. Psaila, R.N. Kaplan, J.F. Bromberg, Y. Kang, M.J. Bissell, T.R. Cox, A.J. Giaccia, J.T. Erler, S. Hiratsuka, C.M. Ghajar, D. Lyden, Pre-metastatic niches: organ-specific homes for metastases, Nat Rev Cancer 17(5) (2017) 302-317.
[32] A. Hoshino, B. Costa-Silva, T.L. Shen, G. Rodrigues, A. Hashimoto, M. Tesic Mark, H. Molina, S. Kohsaka, A. Di Giannatale, S. Ceder, S. Singh, C. Williams, N. Soplop, K. Uryu,

L. Pharmer, T. King, L. Bojmar, A.E. Davies, Y. Ararso, T. Zhang, H. Zhang, J. Hernandez, J.M. Weiss, V.D. Dumont-Cole, K. Kramer, L.H. Wexler, A. Narendran, G.K. Schwartz, J.H. Healey, P. Sandstrom, K.J. Labori, E.H. Kure, P.M. Grandgenett, M.A. Hollingsworth, M. de Sousa, S. Kaur, M. Jain, K. Mallya, S.K. Batra, W.R. Jarnagin, M.S. Brady, O. Fodstad, V. Muller, K. Pantel, A.J. Minn, M.J. Bissell, B.A. Garcia, Y. Kang, V.K. Rajasekhar, C.M. Ghajar, I. Matei, H. Peinado, J. Bromberg, D. Lyden, Tumour exosome integrins determine organotropic metastasis, Nature 527(7578) (2015) 329-35.

[33] M.A. Matthay, R.L. Zemans, The acute respiratory distress syndrome: pathogenesis and treatment, Annu. Rev. Pathol. 6 (2011) 147-63.

[34] L.M. Salazar, A.M. Herrera, Fibrotic response of tissue remodeling in COPD, Lung 189(2) (2011) 101-9.

[35] K. Takeuchi, K. Matsumoto, M. Furuta, S. Fukuyama, T. Takeshita, H. Ogata, S. Suma, Y. Shibata, Y. Shimazaki, J. Hata, T. Ninomiya, Y. Nakanishi, H. Inoue, Y. Yamashita, Periodontitis Is Associated with Chronic Obstructive Pulmonary Disease, J Dent Res 98(5) (2019) 534-540.

[36] S. Hobbins, I.L. Chapple, E. Sapey, R.A. Stockley, Is periodontitis a comorbidity of COPD or can associations be explained by shared risk factors/behaviors?, Int. J. Chron. Obstruct. Pulmon. Dis. 12 (2017) 1339-1349.

[37] E. Silk, H. Zhao, H. Weng, D. Ma, The role of extracellular histone in organ injury, Cell Death Dis 8(5) (2017) e2812.

[38] S.T. Abrams, N. Zhang, J. Manson, T. Liu, C. Dart, F. Baluwa, S.S. Wang, K. Brohi, A. Kipar, W. Yu, G. Wang, C.H. Toh, Circulating histones are mediators of trauma-associated lung injury, Am J Respir Crit Care Med 187(2) (2013) 160-9.

[39] M. Bosmann, J.J. Grailer, R. Ruemmler, N.F. Russkamp, F.S. Zetoune, J.V. Sarma, T.J. Standiford, P.A. Ward, Extracellular histones are essential effectors of C5aR- and C5L2-mediated tissue damage and inflammation in acute lung injury, Faseb j 27(12) (2013) 5010-21.

[40] C.A. Barrero, O. Perez-Leal, M. Aksoy, C. Moncada, R. Ji, Y. Lopez, K. Mallilankaraman, M. Madesh, G.J. Criner, S.G. Kelsen, S. Merali, Histone 3.3 participates in a self-sustaining cascade of apoptosis that contributes to the progression of chronic obstructive pulmonary disease, Am J Respir Crit Care Med 188(6) (2013) 673-83.

[41] R. Allam, S.V. Kumar, M.N. Darisipudi, H.J. Anders, Extracellular histones in tissue injury and inflammation, J Mol Med (Berl) 92(5) (2014) 465-72.

[42] R.S. Doster, L.M. Rogers, J.A. Gaddy, D.M. Aronoff, Macrophage Extracellular Traps: A Scoping Review, J Innate Immun 10(1) (2018) 3-13.

578 **Figure legends**

579 Figure 1. ***Porphyromonas gingivalis*-infected (*Pg*-inf) THP-1 cells released EVs.**

580 (A) Schedule of cell culture and EV isolation. (B) S-*Pg* internalization in THP-1 cells detected via
581 western blotting using an antibody against SNAP26b. The extract of S-*Pg* bacterial cells was also
582 applied as a positive control (S-*Pg*). (C) The presence of green fluorescence-labeled *Pg* in the cells was
583 detected by confocal microscopy. The actin filaments and nuclei were stained with Phalloidin (red) and
584 Hoechst 33342 (blue), respectively. (D) The viability of *Pg* within THP-1 cells was determined with
585 blood agar (upper panel) and the quantification of colony-forming units. The data are given as the mean
586 ± standard error of the mean. (n = 4). ** $p < 0.01$ compared with CFU at 4 h (lower panel). (E) The
587 shape of the EVs isolated from the cultured media of THP-1 infected with (*Pg*-inf EVs) or without *Pg*
588 (No-inf EVs). The scale bars indicate 200 nm.

589

590 Figure 2. **EVs of *Porphyromonas gingivalis*-infected (*Pg*-inf) THP-1 cells included histone proteins.**
591 (A) Silver-stained SDS-PAGE gel showing cargo proteins of EVs. EVs derived from noninfected THP-
592 1 cells (No-inf EVs, lane 1), *Pg* infected THP-1 cells (*Pg*-inf EVs, lane 2), and bacterial cells of *Pg* (*Pg*,
593 lane 3) are shown. M means molecular marker. The arrows (a-c) indicate low molecular proteins in *Pg*-
594 inf EVs. (B) Immunofluorescence microscopy images of THP1 cells stained with histone H3 antibody
595 (green). The arrowheads indicate histone H3 leaking. The scale bars indicate 10 μm. (C) The levels of
596 histone H3 protein were analyzed using western blotting. The cell lysate and EVs from THP1 cells
597 infected with (*Pg*-inf) or without *Pg* (No-inf) are shown. The bacterial cells of *Pg* are also shown as *Pg*.
598 The levels of β-actin and CD9 are shown as a loading control and marker of EVs, respectively. (D) The
599 concentration of histone H3 in EVs. The data are given as the mean ± standard error of the mean. (n =
600 4). * $p < 0.05$ compared with No-inf EVs. (E) The cell lysates from *Pg*-infected THP1 cells pretreated
601 with (*Pg* + CytD) or without cytochalasin D (*Pg*) were spread on blood agar (upper panel). The colonies
602 on blood agar were quantified as colony forming units (lower panel). The data are given as the mean ±
603 standard error of the mean. (n = 4). * $p < 0.05$ compared with *Pg* infected THP1 cells without

cytochalasin D. (G) The levels of histone H3 protein in EVs from THP-1 cells infected with *Pg* in the presence of cytochalasin D.

Figure 3. **EVs of THP-1 cells translocated to multiple organs in mice.**
(A) EV protein (15 μg) derived from *Pg* (*Pg*-inf EVs) or noninfected (No-inf EVs) THP-1 cells or PBS were labeled with Cy7 and injected into mice intraperitoneally. At 2 h post-injection, various organs were dissected and Cy7 fluorescence was detected using the IVIS Spectrum imaging system. The color scale indicates radiant efficiency (Min = 4.26×10^7 and Max = 1.51×10^8). (B) *Pg*-infected EVs derived from THP-1 cells (THP-1), mouse osteoblasts (MC3T3), human gingival epithelial cells (TR146), human hepatocyte (HepG2), and PBS were labeled with Cy7 and injected into the mice intraperitoneally; Cy7 fluorescence was detected using the same procedure as shown in A. The color scale indicates radiant efficiency (Min = 2.89×10^7 and Max = 1.63×10^8).

Figure 4. ***Porphyromonas gingivalis*-infected (*Pg*-inf) EVs induced pulmonary injury in mice.**
The mice were intraperitoneally injected with EVs derived from *Pg* (*Pg*-inf EVs) or non-infected (No-inf EVs) THP-1 cells or PBS (negative control), and then the lungs were removed at 4 h post-injection. (A) H&E staining of the lungs from mice injected with PBS (a), *Pg*-inf EVs (b, d, e, f), or No-inf EVs (c). The asterisks indicate edema and arrowheads indicate blood congestion (d). Photomicrographs of fibrinogen (e) or rabbit IgG (f) stained lung tissue sections from *Pg*-inf EV-treated mice; scale bars indicate 100 μm (a-c), 20 μm (d), or 50 μm (e, f). (B) Immunofluorescence microscopy of the lungs stained with neutrophil elastase (red) (a, b) or normal rabbit IgG (c) from mice injected with PBS (a) or *Pg*-inf EVs (b, c). Nuclei were stained with Hoechst 33342 (blue). Scale bars indicate 10 μm.

The mice were intraperitoneally injected with *Pg*-inf EVs, No-inf EVs, or PBS (negative control) for 12 weeks. (C) Mice were injected with XenoLight RediJect Inflammation Probe, and luminescence in the organs was monitored using the IVIS spectrum imaging system at 10 min post-injection. The color scale indicates radiant efficiency (Min = 4.41×10^7 and Max = 9.14×10^7). (D) The mRNA levels

of inflammation-related genes in the lung tissue were analyzed using qPCR. * $p < 0.05$, ** $p < 0.01$ compared with PBS-treated mice (n = 5). (E) H&E staining (a, b) or Masson's trichrome staining (c, d) of the lungs of mice injected with PBS or *Pg*-inf EVs. "br" means bronchiole and "v" means small blood vessels. Arrows indicate collagen accumulation, and arrowheads indicate broken alveoli (b, d). Scale bars indicate 50 μm.

Figure 5. **Histone H3 in *Porphyromonas gingivalis*-infected (*Pg*-inf) EVs increased inflammatory cytokines via the NF-κB pathway in A549 cells.**

(A) A549 cells were treated with *Pg*-inf EVs or No-inf EVs for 4 h. The mRNA expressions were analyzed using real-time PCR. (B) The mRNA expressions were analyzed using real-time PCR in *Pg*-inf EVs-treated A549 cells in the presence of NF-κB inhibitor, BAY. (C) Western blot analysis of the proteins that regulate NF-κB signaling in *Pg*-inf EVs-treated A549 cells. (D) The p65 subunit was stained with p65 antibody (a, b, and g) or normal rabbit IgG (c). Nuclei were stained with Hoechst 33342 and then microscopic images were merged (d, e, f, and h). (E) *Pg*-inf EVs were treated with or without trypsin. The levels of histone H3 were detected using western blot analysis (upper panels, EVs). A549 cells were treated with *Pg*-inf EVs or trypsin-digested *Pg*-inf EVs for 60 min, then p65 phosphorylation was detected (lower panels, A549). (F) A549 cells were treated with *Pg*-inf EVs or trypsin-digested *Pg*-inf EVs for 4 h, and the mRNA expression was measured using real-time PCR. The data are given as the mean ± standard error of the mean (n = 4). ** $p < 0.01$ compared with each control group.

Supplementary Figure legends

Supplementary Figure 1. ***Pg* treatment did not induce host cell death in THP-1 cells.**

(A) The morphology of *Pg*-treated THP-1 cells. (B). The PI-positive cells were observed using microscopy in THP-1 cells at 48 h post *Pg* or *F. nucleatum* treatment (upper panel). The ratio of PI-positive cells in all Hoechst stained cells is shown in the lower panel. The data are given as the mean ±

656 standard error of the mean. (n = 4). (C) Lactate dehydrogenase (LDH) release was measured in the same
657 cells in B. The data are given as the mean ± standard error of the mean. (n = 4).
658
659 Supplementary Figure 2. **Measurement of particle size of EVs.**
660 The diameter of EVs from the *Pg* infected THP-1 cells (*Pg*-inf EVs) or noninfected THP-1 cells (No-
661 inf EVs) were measured using a Zetasizer. The means of the particle diameter of the No-inf EVs and
662 *Pg*-inf EVs were 198.2 nm and 199.8 nm, respectively
663
664 Supplementary Table 1. **EVs proteins are identified by mass spectrometry.**
665 Three bands corresponding to the low-molecular-weight proteins shown in figure 2A (a–c) were
666 identified as multiple core histones including histone H2A, H2B, H3, and H4 using Nano-LC-MS/MS.
667
668 Supplementary Figure 3. **Analysis of EVs released from *Pg*-infected non-phagocytic cells.**
669 Mouse osteoblasts (MC3T3), human gingival epithelial cells (TR146), and human hepatocytes (HepG2)
670 were infected with green fluorescent-labeled *Pg* for 4 h. (A). The invaded *Pg* inside the cells was
671 observed using confocal microscopy. (B). The non-phagocytic cells shown as A were infected with *Pg*,
672 and then EVs were isolated from the cultured media at 48 h post-infection. The diameter of the EVs
673 was measured using a Zetasizer. The mean particle diameter was 40.92 nm in MC3T3-E1 cells; 64.84
674 nm in TR cells; 83.89 nm in HepG2 cells.
675
676 Supplementary Figure 4. **Recombinant histone H3 increased inflammatory cytokines via the NF-**
677 **κB pathway in A549 cells.**
678 (A). A549 cells were treated with recombinant human histone H3 for 4 h, and then mRNA expressions
679 were analyzed using real-time PCR. (B). The mRNA expressions were analyzed using real-time PCR
680 in recombinant histone H3-treated A549 cells in the presence of NF-κB inhibitor, BAY. The data are

given as the mean ± standard error of the mean (n = 4). * $p < 0.05$, ** $p < 0.01$ compared with each control group.

Supplementary Figure 5. **Our proposal model.**

In periodontitis, macrophages are infected with *Pg*, periodontal bacteria (A), and released extracellular vesicles (EVs) which included histone H3 (B). These EVs translocated to the lungs through blood circulation, and there histone H3 induced cytokines by NF-kB pathways (C), resulting in pulmonary injury such as edema, vascular congestion and collagen deposition (D).

Figure 1. ***Porphyromonas gingivalis*-infected (*Pg*-inf) THP-1 cells released EVs.**

A

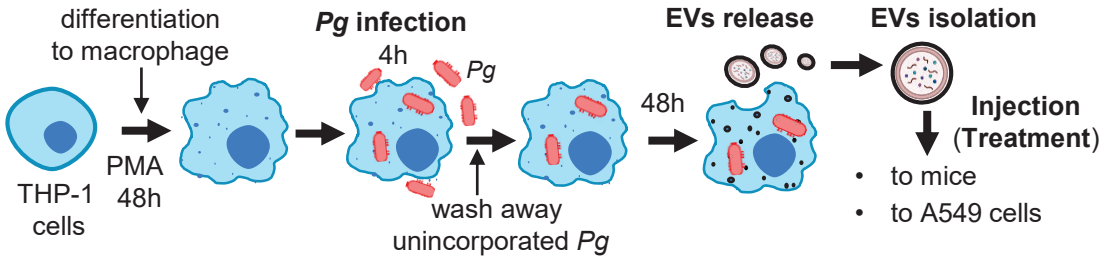

B

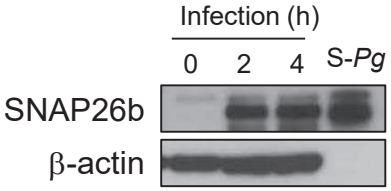

C

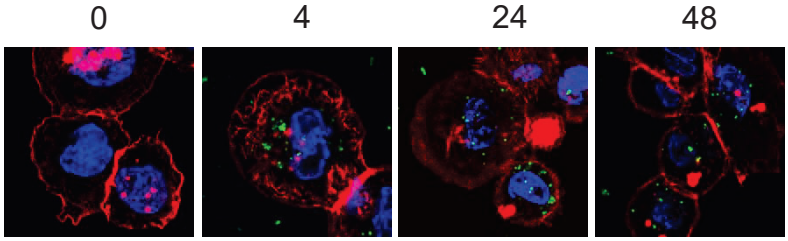

D

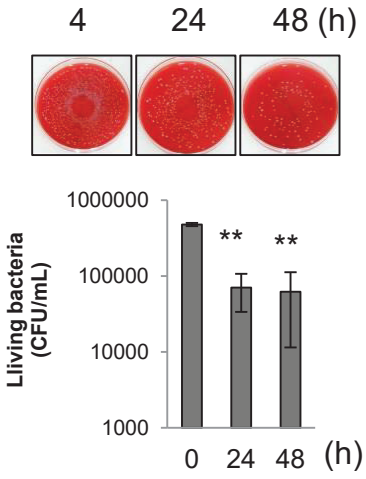

E

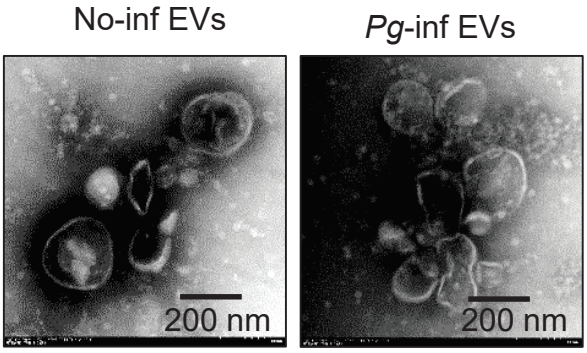

Figure 2. EVs of *Porphyromonas gingivalis*-infected (*Pg*-inf) THP-1 cells included histone proteins.

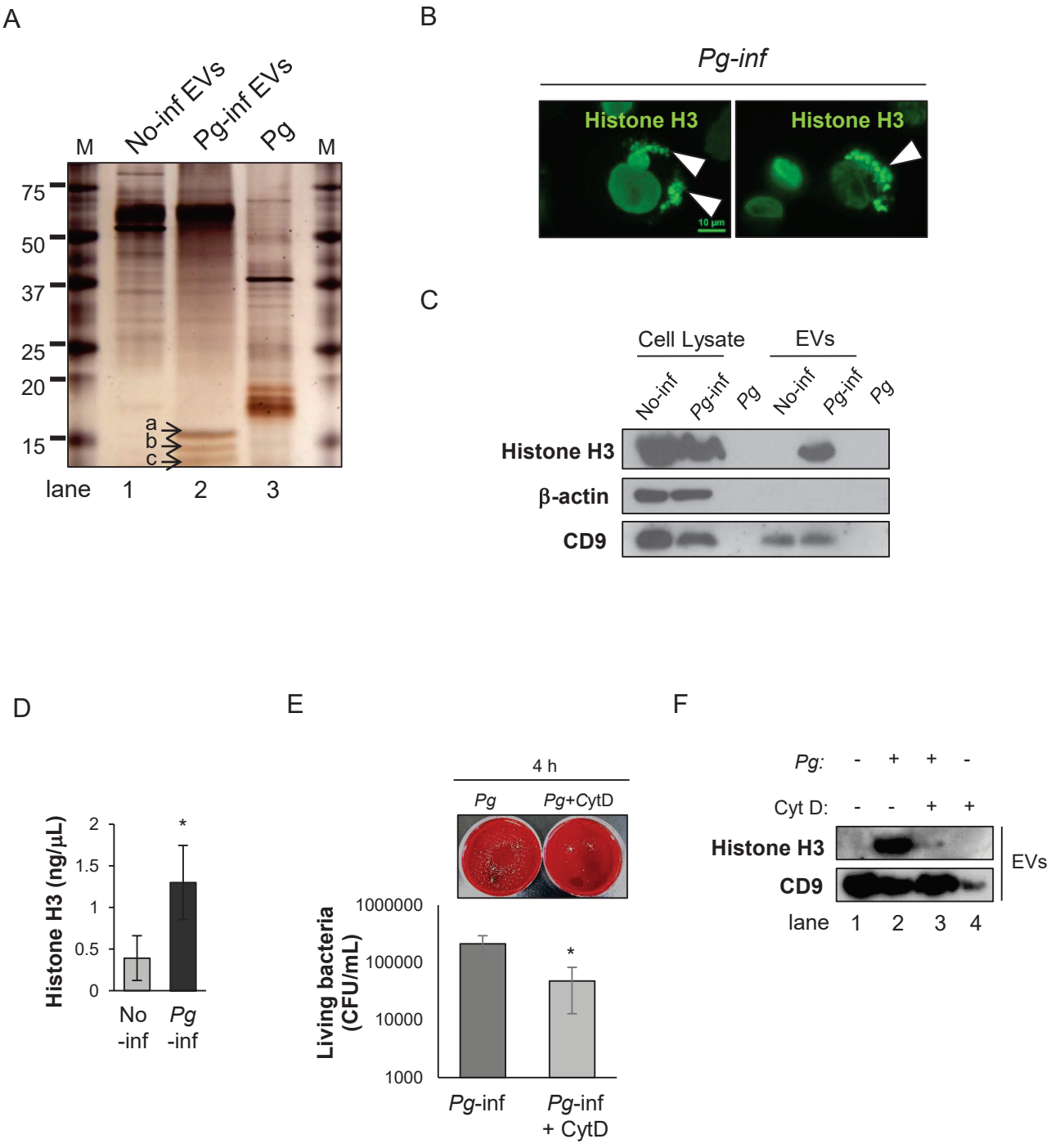

Figure 3. EVs of THP-1 cells translocated to multiple organs in mice.

A

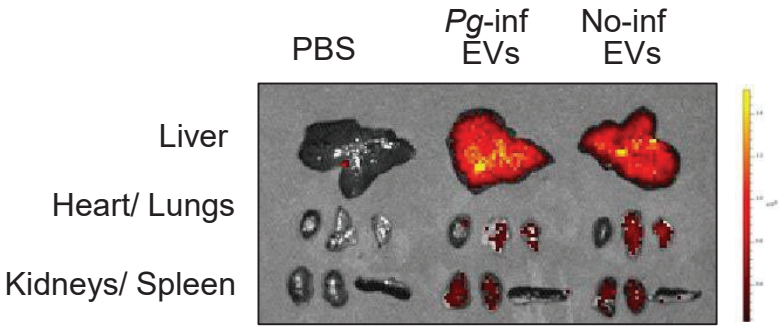

B

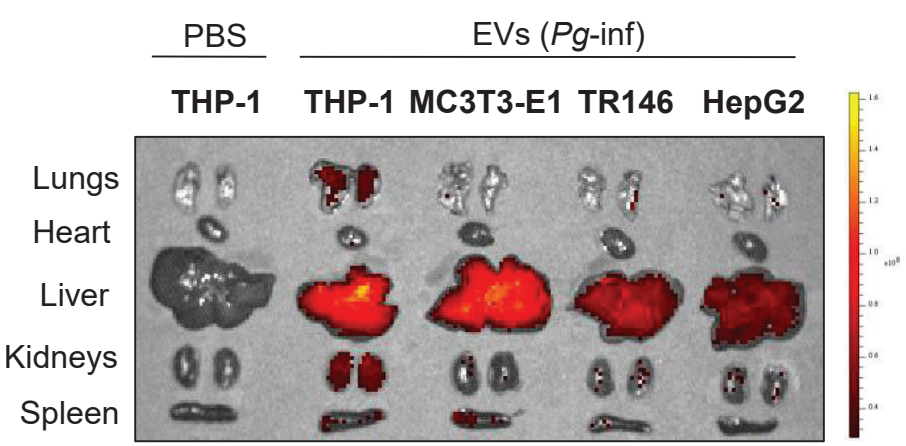

Figure 4. *Porphyromonas gingivalis*-infected (*Pg*-inf) EVs induced pulmonary injury in mice.

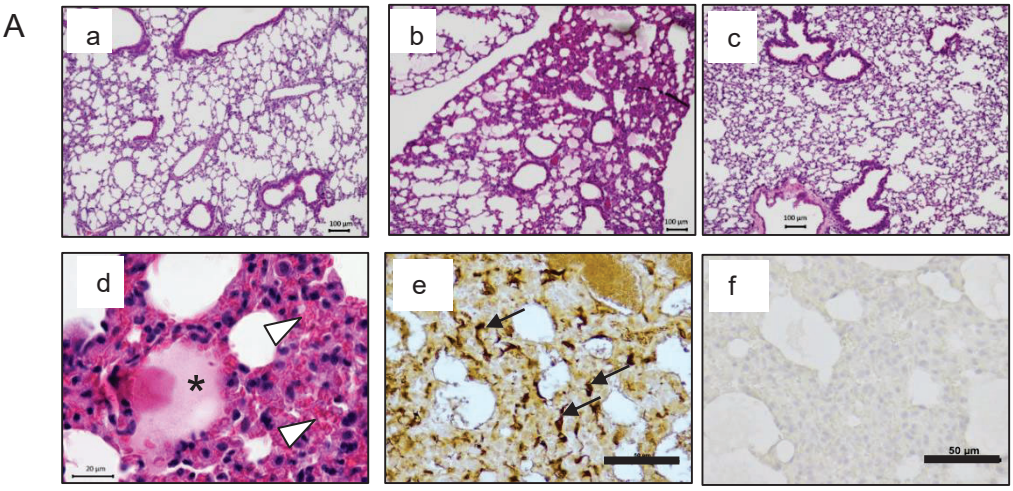

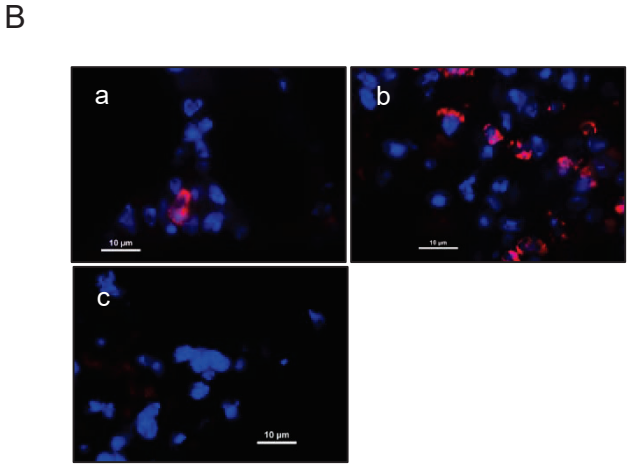

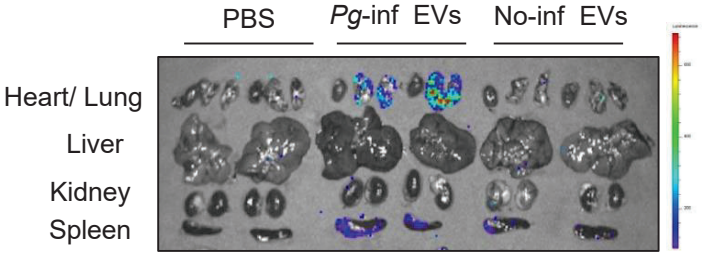

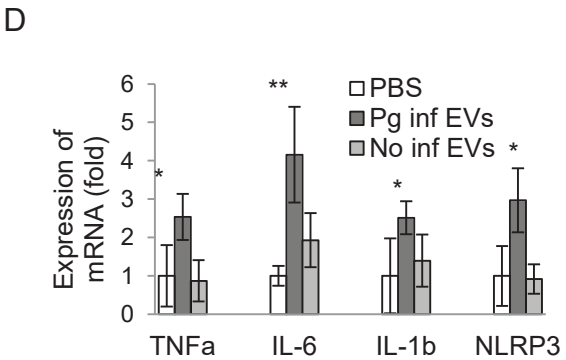

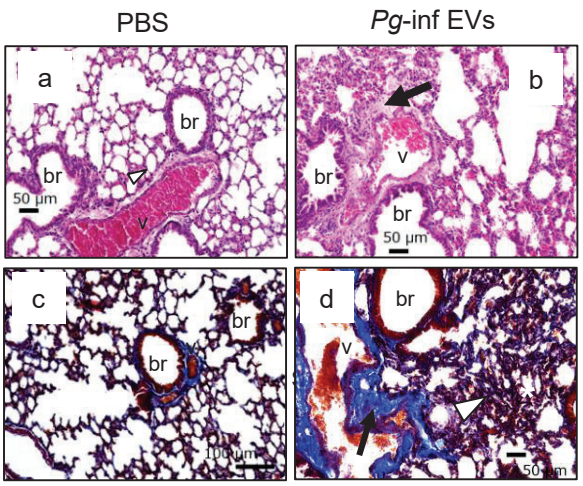

Figure 5. Histone H3 in *Porphyromonas gingivalis*-infected (*Pg*-inf) EVs increased inflammatory cytokines via the NF-κB pathway in A549 cells.